SIMULTANEOUS RECONSTRUCTION AND SEGMENTATION ALGORITHM FOR POSITRON EMISSION TOMOGRAPHY AND TRANSMISSION TOMOGRAPHY

D. Van de Sompel, M. Brady

University of Oxford
Department of Engineering Science
Parks Road, Oxford OX1 3PJ, UK

ABSTRACT

We present a new reconstruction algorithm for emission and transmission tomography. The algorithm performs maximum likelihood reconstruction and doubly stochastic segmentation simultaneously. The resulting reconstructions show promising edge-preservation as well as suppression of measurement noise.

Index Terms— Image reconstruction, maximum likelihood estimation, image segmentation, positron emission tomography, transmission tomography.

1. INTRODUCTION

The literature on positron emission tomography, transmission tomography, limited angle CT, and, most recently, digital breast tomosynthesis contains a myriad of reconstruction algorithms. Each of these algorithms embodies a unique set of assumptions, and yields reconstructions of varying quality depending on the application. Perhaps the most common reconstruction algorithm is the filtered backprojection (FBP) algorithm, first proposed by Bracewell and Riddle in the context of radioastronomy [1]. The major advantage of FBP is its linearity and noniterative nature, which makes it computationally efficient. Unfortunately, FBP yields streaky reconstructions in the presence of measurement noise. In the case of incomplete angular sampling, it also suffers from an underrepresentation of low frequency content (resulting in low contrast for larger masses), an inability to respect object support, and the generation of additional streak artifacts. While several filter designs have been proposed to alleviate these problems [2, 3], the use of FBP in emission tomography and limited angle transmission tomography inevitably leads to reconstructions that are streaky and, to varying extents, unfaithful to the original projection data.

Most alternative algorithms fall in the category of iterative reconstruction algorithms, which includes algebraic reconstruction (ART) algorithms [4] and penalized maximum likelihood (PML) algorithms [5]. While faithful to the projection data, algebraic reconstruction techniques offer only limited noise and image modeling opportunities. As a result, they perform poorly in the presence of measurement noise. PML reconstruction techniques allow for more advanced image and noise modeling: by imposing local MRF constraints, solutions can be easily regularized. To our knowledge, most previous work on PML reconstruction has applied such constraints to pixel intensities, using either quadratic or alternative, edge-preserving penalty functions [6, 7]. A notable exception is [8], which uses a hybrid level set (nonlocal) and MRF (local) approach to estimate region boundaries and pixel intensities simultaneously. In this work, we will apply a local spatial coherence constraint to the *class labels* of object pixels, and develop a new simultaneous reconstruction and segmentation (SRS) algorithm. The algorithm can be used for both emission and transmission tomography, where the latter includes applications such as limited angle CT and tomosynthesis.

2. METHODS

2.1. Objective Function

Our objective is to maximize the joint posterior probability $P(x, p, \theta|r)$, where p is the hidden Markov measure field proposed by Marroquin [9], x is the attenuation or concentration map of the imaged object, r is the observed projection data (photon counts), and θ is a vector containing the model parameters that characterize the tissue classes or concentration levels in the object. Using Bayes' rule and the definition of conditional probability, the posterior probability can be decomposed as

$$P(x, p, \theta|r) = \frac{1}{Z_r} P(r|x)P(x|p, \theta)P(p)P(\theta) \qquad (1)$$

where we have assumed a uniform distribution for the projection data r, and $P(r|p, x, \theta) = P(r|x)$ since the projection data depends only on the object's attenuation or concentration map.

The data likelihood term $P(r|x)$ is different for emission and transmission tomography. Conveniently, however, the data likelihood can in both cases be expressed in the following general form:

$$\log P(r|x) = \sum_{i=1}^{M} h_i(l_i) + \text{constant} \tag{2}$$

where each $h_i(l_i)$ is a concave function. In the case of emission tomography, $h_i(l_i)$ is given by

$$h_i(l_i) = -(l_i + b_i) + r_i \log(l_i + b_i) \tag{3}$$

where $l_i = \sum_{j=1}^{N} a_{ij} x_j$. The N-dimensional vector x is the emission density of the object, a_{ij} is the probability that a photon emitted by pixel j is detected by the i^{th} detector pair, r_i is the photon count observed by the i^{th} detector pair, and b_i denotes background events such as random coincidences and scatter. In the case of transmission tomography, $h_i(l_i)$ is given by

$$h_i(l_i) = -\left(r_0 e^{-l_i} + b_i\right) + r_i \log\left(r_0 e^{-l_i} + b_i\right) \tag{4}$$

where $l_i = \sum_{j=1}^{N} a_{ij} x_j$. The N-dimensional vector x is the attenuation map of the object, a_{ij} is the length of traversal of the i^{th} ray through the j^{th} pixel, r_i is the photon count observed by the i^{th} detector, $r_{0,i}$ is the number of photons leaving the source for the i^{th} ray, and b_i accounts for scatter events.

The remaining terms in Eqn. 1 are identical for both emission and transmission reconstruction. Assuming conditional independence of the pixels, we can express the conditional probability $P(x|p, \theta)$ as

$$P(x|p, \theta) = \prod_{j=1}^{N} P(x_j|p, \theta), \tag{5}$$

where

$$P(x_j|p, \theta) = \sum_{k}^{K} v_{j,k} p_{j,k} = v_j \cdot p_j \tag{6}$$

and K is the number of possible classes in the image. The actual class labels f_j of the pixels x_j have been marginalized out as described in Marroquin [9]. The k^{th} entry of the K-dimensional vector p_j gives the prior probability that the j^{th} pixel belongs to the k^{th} class. The k^{th} entry of the vector v_j, in turn, specifies the probability that the j^{th} pixel belongs to the k^{th} class, *given* the current reconstructed pixel intensity x_j and the class parameters θ. Assuming that the intensities of each tissue class follow a Gaussian distribution[1] with mean μ_k and standard deviation σ_k, the probabilities $v_{j,k}$ are written as

$$v_{j,k} = P_{G,\mu_k,\sigma_k}(x_j) = \frac{1}{\sigma_k \sqrt{2\pi}} \exp\left(-\frac{(x_j - \mu_k)^2}{2\sigma_k^2}\right) \tag{7}$$

Next, the prior probability $P(p)$ is subject to a Markov Random Field distribution. In other words, we believe that each vector p_j should be similar to its neighbors. The probability density function is given by the Gibbsian penalty function

$$P(p) = \frac{1}{Z_p} \exp\left[-\sum_{C} V_C(p)\right] \tag{8}$$

where Z_p is a normalizing constant, C denotes the cliques, and V_C is a desirable potential function. Following Marroquin [9], we will use a simple quadratic potential function:

$$V_{r,s}(p_r, p_s) = \lambda \|p_r - p_s\|^2 = \lambda \sum_{k}^{K} (p_{r,k} - p_{s,k})^2 \tag{9}$$

where r and s are neighboring pixels in a given clique, and λ is a hyperparameter determining the strength of the prior.

In this paper, we will assume a uniform distribution for $P(\theta)$. Of course, it is usually possible to formulate a feasible range of values for the parameters θ. We intend to explore the effects of a non-uniform distribution at our next available opportunity.

2.2. Optimization

The expression given by Eqn. 1 can be optimized by maximizing its natural logarithm, yielding the cost function

$$\psi(x, p, \theta) = \log P(r|x) + \log P(x|p, \theta) + \log P(p), \tag{10}$$

where any constant terms have been dropped. Note also that the optimization problem is subject to the nonnegativity constraint for x, and the simplex constraint for p:

$$p_j \in S_K = \left\{ p_j \in \mathbb{R}^K : \sum_{k=1}^{K} p_{j,k} = 1, p_{j,k} \geq 0, k = 1, ..., K \right\} \tag{11}$$

In the design of our algorithm, we pursue the following strategy for maximizing $\psi(x, p, \theta)$:

1. initialize x, p, and θ
2. holding p, θ fixed, optimize over x (image update)
3. holding x, θ fixed, optimize over p (measure field update)

[1] Of course, alternative variation models are possible as well. In other words, the SRS framework allows us to model the intensity variations within each tissue class explicitly.

4. holding x, p fixed, optimize over θ (parameter update)

The proposed algorithm will cycle between steps 2, 3 and 4, until convergence is reached[2]. The completion of one such cycle will constitute one iteration of the algorithm.

1) Image update

With p,θ fixed, we would like to maximize the following cost function over x:

$$\psi(x) = \sum_{i=1}^{M} h_i(l_i) + \sum_{j=1}^{N} \log(v_j \cdot p_j) \tag{12}$$

The first term can be approximated by parabolas of an optimal curvature [10, 11]. The second term is more difficult to handle, since it consists of the log of a weighted sum of Gaussian distributions. We can simplify the problem by approximating this Gaussian mixture model by its first and second moments. This yields a single Gaussian distribution with the following mean and standard deviation:

$$\mu_j^* = \sum_{k=1}^{K} p_{j,k}\mu_k \tag{13}$$

and

$$\sigma_j^* = \sqrt{\left[\sum_{k=1}^{K} p_{j,k}(\sigma_k^2 + \mu_k^2)\right] - (\mu_j^*)^2} \tag{14}$$

Conveniently, this approximation turns the second term into a simple parabola, which can be dealt with very easily. Note that the approximation becomes more accurate as the weighted sum of Gaussian becomes dominated by one of the component Gaussians. The cost function has become

$$\begin{aligned} \psi(x) &\approx \sum_{i=1}^{M} h_i(l_i) + \sum_{j=1}^{N} \log(P_{G,\mu_j^*,\sigma_j^*}(x_j)) \\ &= \sum_{i=1}^{M} h_i(l_i) + \sum_{j=1}^{N} \left[\log\left(\frac{1}{\sigma_j^*\sqrt{2\pi}}\right) - \frac{(x_j - \mu_j^*)^2}{2(\sigma_j^*)^2} \right] \\ &= \phi(x) \end{aligned} \tag{15}$$

Minorizing the first term on the right hand side as mentioned above, we obtain

$$\begin{aligned} \phi(x) &\geq \sum_{i=1}^{M} q_i(l_i; l_i^n) + \sum_{j=1}^{N} \left[\log\left(\frac{1}{\sigma_j^*\sqrt{2\pi}}\right) - \frac{(x_j - \mu_j^*)^2}{2(\sigma_j^*)^2} \right] \\ &= Q(x; x^n) \end{aligned} \tag{16}$$

[2]Note that the algorithm cannot guarantee convergence onto a global optimum - it may converge to a local maximum.

where $q_i(l_i; l_i^n) = h_i(l_i^n) + \dot{h}_i(l_i^n)(l_i - l_i^n) + \frac{1}{2}c_i(l_i^n)(l_i - l_i^n)^2$, and x^n denotes the image estimate at the beginning of the n^{th} iteration. The optimal curvatures were given by Erdogan and Fessler [10, 11] as

$$c_i(l_i^n) = \begin{cases} \left[2\frac{h_i(0) - h_i(l_i^n) + \dot{h}_i(l_i^n)l_i^n}{(l_i^n)^2}\right]_-, & l_i^n > 0 \\ \left[\ddot{h}_i(0)\right]_-, & l_i^n = 0, \end{cases} \tag{17}$$

which yields a parabola tangent at l_i^n that intersects the original h_i function at $l_i = 0$. The cost function (16) can be optimized efficiently using a sequential Newton-Raphson coordinate ascent method.

2) Measure field update

Here, we would like to maximize the following cost function over p:

$$\begin{aligned} \psi(p) &= \sum_{j=1}^{N} \log(v_j \cdot p_j) - \sum_{C} V_C(p) \\ &= \sum_{j=1}^{N} \log(v_j \cdot p_j) - \lambda \sum_{j=1}^{N} \left\{ \sum_{i=1}^{I} \left(c_i \sum_{k=1}^{K} (p_{j,k} - p_{\tilde{j}_i,k})^2 \right) \right\} \end{aligned} \tag{18}$$

where c_i gives the weight associated with the ith neighbor in the clique (in this study each clique contained 8 pixels), and $\tilde{j}_i$ identifies the ith neighbor of pixel j. The weights c_i associated with any neighbors that fall outside of the image domain are set to zero.

The above optimization problem is similar to the problem faced in [9], and can be solved using the Gradient Projection Newtonian Ascent approach outlined therein.

3) Parameter update

In this step, we aim to maximize the following cost function over θ:

$$\psi(\theta) = \sum_{j=1}^{N} \log(v_j \cdot p_j) \tag{19}$$

This was achieved using the Gradient Projection Newtonian Ascent method as well.

3. RESULTS

In applications such as limited angle CT, it is conceivable that the natural variations in tissue attenuation properties are known *a priori*. This allows us to set the parameter vector θ accordingly, and to skip the parameter update. Here, we will illustrate the results of such reconstructions using a simple piecewise constant phantom, where the standard deviations have been set to some

(a) original

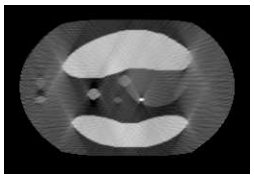

(b) FBP initialization (noiseless projections)

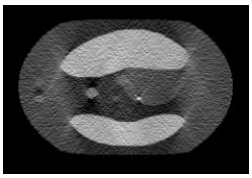

(c) FBP initialization (projections with Poisson noise)

(d) SRS reconstruction from noiseless projections

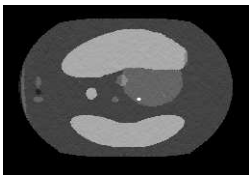

(e) SRS reconstruction, Poisson noise

Fig. 1. SRS reconstructions from (d) noiseless and (e) noisy (Poisson, 15,000 incident photons) projections.

small number. Fig. 1(d) shows a near-perfect reconstruction from 50 noiseless views with a missing angular range of 60^o (missing $\pm 30^o$ about the x-axis). Fig. 1(e) shows the same reconstruction from noisy views, where the noise was Poisson distributed, and the number of incident photons along each ray was 15,000.

Due to space limitations, we only present results in 2D. The extension to three dimensions is however straightforward. We plan to report more extensive results for limited angle CT, as well as emission tomography and digital breast tomosynthesis, at our next opportunity. There, we will explore how factors such as hyperparameter relaxation, number of views, noise level, and angular range affect the reconstruction quality.

4. CONCLUSION

We have developed an algorithm that uses doubly stochastic segmentation to guide maximum likelihood reconstruction in emission and transmission tomography. The algorithm shows promising edge preservation and noise suppression properties.

We are currently exploring the algorithm's robustness when the parameter values are not known *a priori*, i.e. when the parameters θ have to be estimated along with x and p during the course of the reconstruction.

5. REFERENCES

[1] R.N. Bracewell and A.C. Riddle, "Inversion of fan-beam scans in radio astronomy," *Astrophys. J.*, vol. 150, pp. 427–434, Nov 1967.

[2] G. Lauritsch and W. Haerer, "A theoretical framework for filtered backprojection in tomosynthesis," *SPIE Conference on Image Processing*, vol. 3338, pp. 1127–1137, February 1998, San Diego, California.

[3] J. Orman, T. Mertelmeier, and W. Haerer, "Adaptation of image quality using various filter setups in the filtered backprojection approach for digital breast tomosynthesis," *International Workshop for Digital Mammography 2006*, vol. 4046, pp. 175–182, 2006.

[4] A.C. Kak and M. Slaney, *Principles of Computerized Tomographic Imaging*, Society of Industrial and Applied Mathematics, 2001.

[5] K. Lange and R. Carson, "Em reconstruction algorithms for emission and transmission tomography.," *J. Comput. Assist. Tomog.*, vol. 8, pp. 306–316, 1984.

[6] J.A. Fessler, "Iterative methods for image reconstruction," EECS Department, The University of Michigan, ISBI Tutorial, April 6, 2006.

[7] A.H. Delaney and Y. Bresler, "Globally convergent edge-preserving regularized reconstruction: an application to limited-angle tomography," *Image Processing, IEEE Transactions on*, vol. 7, no. 2, pp. 204–221, 1998.

[8] D.F. Yu and J.A. Fessler, "Edge-preserving tomographic reconstruction with nonlocal regularization," *Medical Imaging, IEEE Transactions on*, vol. 21, no. 2, pp. 159–173, Feb 2002.

[9] J.L. Marroquin, E.A. Santana, and S. Botello, "Hidden markov measure field models for image segmentation," *IEEE transactions on Pattern Analysis and Machine Intelligence*, vol. 25, no. 11, pp. 1380–1387, November 2003.

[10] H. Erdogan and J.A. Fessler, "Accelerated monotonic algorithms for transmission tomography," in *ICIP (2)*, 1998, pp. 680–684.

[11] J.A. Fessler and H. Erdogan, "A paraboloidal surrogates algorithm for convergent penalized-likelihood emission image reconstruction," *Nuclear Science Symposium, 1998. Conference Record. 1998 IEEE*, vol. 2, pp. 1132–1135 vol.2, 1998.